EasyChair Preprint

№ 3922

Design and Prototype of a Sensor-Based and Battery-Powered Inline Robot for Water Quality Monitoring in Water Distribution Systems

Saber Kazeminasab, Mohsen Aghashahi and M. Katherine Banks

July 21, 2020

Design and Prototype of a Sensor-Based and Battery-Powered Inline Robot for Water Quality Monitoring in Water Distribution Systems

Saber Kazeminasab, Mohsen Aghashahi, and M. Katherine Banks

***Abstract*— Water distribution systems are critical infrastructures that are expected to supply healthy water. Deliberate or accidental incidents such as terrorist attacks or pipe breaks can contaminate potable water in pipelines. Inline mobile sensors are promising solutions which have been designed and developed to monitor water quality and detect leaks in water pipelines. These mobile sensors can move towards the location of contamination or leak and provide more timely and accurate measurements. However, these sensors, which are often free-swimming spheres and move by water flow, have two problems: instability and passiveness. In this research, we designed a robot that stabilizes and automates our previously fabricated spherical mobile sensor. The robot empowers a water utility operator to control the mobile sensor motion in a pressurized environment with a high-speed flow. The robot has three spring-based adjustable arms for stability in pipes with diameters between 22.86 (cm) — 9 (in) and 55.88 (cm) — 22 (in). Each arm is actuated with a motor and a wheel at its end. The wheels are in contact with a pipe wall, and the motors keep the robot moving. Each motor is customized with a gearhead that provides required torque at its wheel for motion. A lithium battery attached to the sphere supplies electricity for motors and sensors. The proposed design is characterized and prototyped in this paper. To evaluate the controllability and observability of the robot, we have linearized governing equations. Results show the successful performance of the robot in pipes.**

I. INTRODUCTION

Water distribution systems (WDSs) are critical infrastructures that transfer drinking water to consumers. In the U.S. about 42 billion gallons of water per day are being delivered via one million miles of pipes to be used in daily life, factories, and offices across the country [1]. The U.S. Environmental Protection Agency (EPA) has set regulations that enforce drinking water utilities to limit the levels of contaminants in drinking water [2]. These contaminants can be introduced to water pipes by accidental or deliberate incidents.

Moreover, aging water infrastructure [3]-[5] has experienced an increase in the break rate [6]. One of the significant consequences of pipe breaks is negative pressure at cross-connections where surrounding non-potable substances come to contact with the potable water in a pipeline and cause public health crises. EPA reported 9,734 water-borne diseases due to cross-connections between 1981 to 1998 [7]. EPA requires water utilities to monitor their potable water supplies by regularly water sampling and laboratory analyses to ensure the drinking water standards are met [8]. These laboratory-based methods, however, are too slow and are not efficient for contamination detection and response in real-time [9]. Though stationary water quality sensors (placed outside of a pipe with their probes measuring flowing water quality) are recommended tools for on-line monitoring, establishing a ubiquitous network of these sensors is burdensome due to their expensive deployment and maintenance [10]. The cost challenges have set a constraint on the number of stationary sensors that can be placed at a network. This problem prevents a water utility from having a stationary sensing network with good spatiotemporal coverage along pipelines. Inline free-swimming sensors that move in a pipe with flowing water have emerged as stand-alone or complementary solutions for real-time water quality monitoring [11],[12], or leak detection in water pipelines [13],[14]. These mobile sensors can be useful when a water quality abnormality or leak is reported in pipe segments that are not monitored by stationary sensors. In this case, an operator can insert a free-swimming sensor from a fire hydrant into a suspicious water pipeline, and it rolls through the desired location for more accurate measurement and monitoring. However, the employment difficulties of these mobile sensors are twofold: i) the sensors disrupt a water network normal operation [15] and ii) random path that each sensor may take at junctions depending on flow conditions [14],[16]. To implement free-swimming sensors, a water utility should stop its network operation and manipulate valves and pumps to deliver a sensor to the desired location. This problem adversely affects network performance and also makes water utilities reluctant to employing the sensors. Moreover, due to the absence of enough control over the sensor motion in a pipe, their temporal or permanent loss have been reported by utilities [17].

Inline robots have been developed and deployed for pipe inspection. They can move in a controlled manner and are either tethered, i.e., connected to an external source with a cable for power supply and data transceiving, or self-powered, that carry a battery for electric devices. Table I includes information about some of the inline robots that have been developed mainly for pipe inspection. We have evaluated their capabilities of being employed for water quality monitoring in a water network. The column Drawback in Table I explains what a robot lacks for water quality measurement applications.

Shao *et al*. [18] compared active and passive in-pipe robots and reported wall-press robots as the most efficient designs for inline robots due to their great vertical mobility, diameter adaptability, stability, driving capacity, and wireless control capability.

Saber Kazeminasab is with the Electrical and Computer Engineering Department, Texas A&M University, TX, USA (saberkazemi1992@tamu.edu).

Mohsen Aghashahi is with the Civil and Environmental Engineering Department, Texas A&M University, TX, USA (aghashahi@tamu.edu).

M. Katherine Banks is with the College of Engineering, Texas A&M University, TX, USA (k-banks@tamu.edu).

TABLE I: EXISTING INLINE ROBOTS CAPABLE OF BEING EMPLOYED IN THE MOBILE WATER QUALITY MONITORING APPLICATION

Author/Company	Name	Application	Sensor Device	Power Supply	Drawback
Qu et al.	Smart-Spider [19]	Offshore oil and gas pipeline inspection	Camera	Self-powered	The authors used Wi-Fi communication that does not work for underground applications.
Kwon and Yi	[20]	Pipeline inspection	Camera	Tethered	The cable-based design of the robot limits its deployment range and disrupts the operation of a network.
Moghaddam and Jerban	[21]	Pipeline inspection	N/A[a]	N/A[a]	The power supply has not been designed and discussed.
Kakogawa and Ma	[22]	Pipeline inspection	Camera	Tethered	The robot is powered with a cable connected to an external battery that disrupts the operation of a network.
Alnaimi et al.	[23]	Pipeline inspection and cleaning	Ultrasonic	Self-powered	The power consumption of electric parts is not discussed.
Chatzigeorgiou et al.	[24]	Leak detection	Acoustic	N/A[a]	The robot is free-swimming and can get lost in addition to disruption in network operation
Wahed and Arshad	[25]	Pipeline inspection	Camera	N/A[a]	The power supply has not been included in the robot design.
Pure Technologies	Sahara [26]	Leak and gas detection, pipe inspection	Camera Acoustic	Tethered	The cable-based design of the robot limits its deployment range and disrupts the operation of a network.
Bandala et al.	[27]	Pipeline inspection	Camera	Tethered	The cable-based design of the robot limits its deployment range and disrupts the operation of a network.

a. Not Available: these characteristics are not available or discussed in the research.

Regarding Table I, the existing inline robots are not well-equipped for application in real-time water quality monitoring in WDSs. Therefore, there is a need for an automated robot that is customized for miniaturized water quality sensors and is capable of operation in a potable water distribution system without disturbing the network services.

Our contributions in this paper are the following:

- A wall-press inline robot is specifically designed for carrying sensing chips in potable water pipelines to measure water quality parameters at desired locations and in a controlled manner. The robot body choice is justified with Computational Fluid Dynamics (CFD) analyses and characterized by the CFD results.
- The robot is equipped with efficient actuators, arms, and springs that enable it to be adjustable and to move in pipelines with different diameters and at junctions. Three customized motors with low-level electricity consumption allow the robot to move more distant and operate for a longer time.
- An efficient battery attached to the robot body makes it independent from cables for the power supply purpose. This capability allows the robot to move in pipelines in or against the direction of flowing water without disturbing the normal operation of water networks.

II. MECHANISM AND COMPONENTS OVERVIEW

The proposed modular robot consists of one sensing and control module, three arm module, and three actuator module (see [a] in Fig. 1). The robot is shown in a pipe as shown in [e] in Fig. 1. In the following, each module is described in detail.

A. Sensing and Control Module

The sphere is composed of two hemispheres (see Fig. 2). One hemisphere, ([c] in Fig. 2), includes a sensing element which can include miniaturized chemical sensors and a micro-pump. The micropump provides water samples by circulating water from the water inlet and outlet holes indicated as ([k] in Fig. 2). This hemisphere is called the sensing hemisphere. the other hemisphere ([j] in Fig. 2), named control hemisphere controls the timing of the operation of the sensor, actuators, the motion control unit, and the wireless communication module Details of the electronic parts are beyond the scope of this paper. In the previous design [28], water could leak into the sphere through the location where the hemispheres were attached. To address this problem, a seal mechanism was designed where a standard off-the-shelf O-ring locates between the hemispheres. Then the hemispheres are fastened with four pairs of screws and nuts which push the O-ring. This sealing design keeps the sphere waterproofed and away from wear and tear. (parts [d], [e], and [f] in Fig. 2), Per arm, there is a basement to attach it to the sphere with ball bearings ([a] and [b] in Fig. 2). Spring anchors connect one end of a spring to the sphere ([g] in Fig. 2). To control arm rotation, there are arm supports on the sphere that prevents the arms from extra rotation ([b] in Fig. 1). The battery ([h] in Fig. 2) power is transmitted to the control hemisphere with wire through a hole ([i] in Fig. 2).

B. Arm Module

Since water networks comprise pipes with different sizes and configurations, an inline robot should be able to adjust its size based on pipe configuration. The designed robot has three arms that are filled and 3D-printed from a photopolymer. The arms have a Boomerang shape so that they do not obstacle the motion of their springs. To maintain the robot balanced, a passive spring was used for each arm.

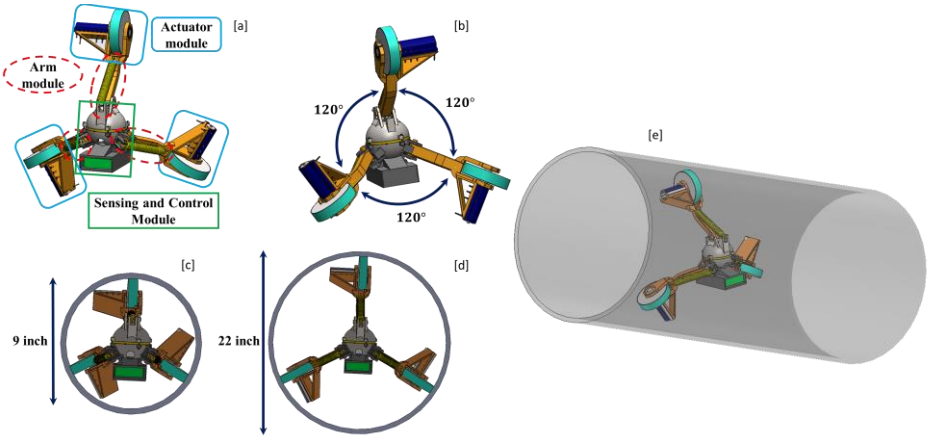

Fig. 1. Overall views of the robot. [a] Front view. [b] Rear view. [c] Minimum robot diameter. [d] Maximum robot diameter. [e] Robot in the pipe.

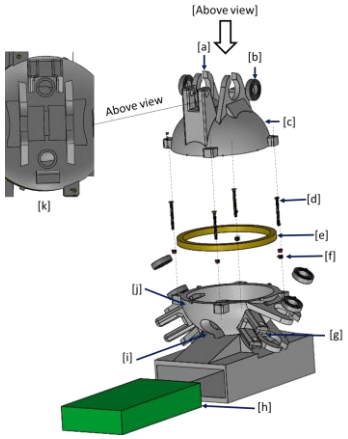

Fig. 2. [a] Arm basement. [b] ball bearing. [c] Sensing hemisphere. [d] Screw. [e] off-the-shelf O-ring. [f] Nut. [g] Spring anchor. [h] Battery. [i] Hole to connect inside and outside of the sphere electrically. [j] Control hemisphere. [k] Water inlet and outlet.

One end of each spring was attached to the sphere via the anchors ([a] in Fig. 2), and another end was connected to the end of the arm (see Fig. 3).

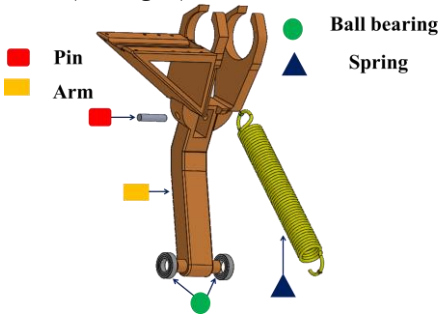

Fig. 3: CAD design of the arm module: exploded view.

The springs provide a required force for arms to be in tension and always keep the wheels in contact with the pipe wall during operation. The arm and spring design allow the robot to be adjustable and to operate in pipes with the diameters range from 9 inch to 22 inch (parts [c] and [d] in Fig. 1).

C. Actuator Module

The actuator module includes a motor cover, a motor, a motor basement, screws and nuts to attach the motor and the motor cover to the motor basement, a gearhead, a wheel, two ball bearings at both sides of the wheel, and a wheel cover made of rubber. Fig. 4 shows the designed actuator module.

The customized electric motors with gearheads are at the end of the arms and fixed on the motor basement (Fig. 4).

To better fix the motors on the basements, the inside surfaces of the motor covers and motor basements were slotted (Fig. 4, (b)). Then these slots and the holes on the motor body were filled with a moldable glue. Not only the moldable glue prevents water from penetrating a motor, but it also increases the friction between the motor cover and motor body.

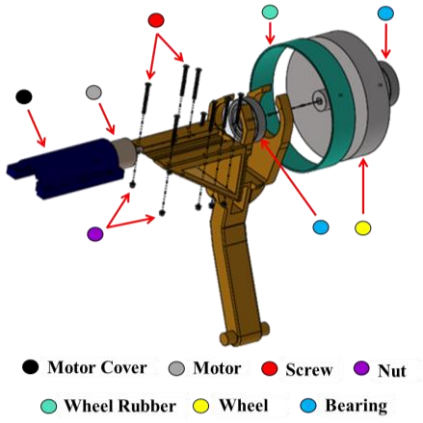

(a)

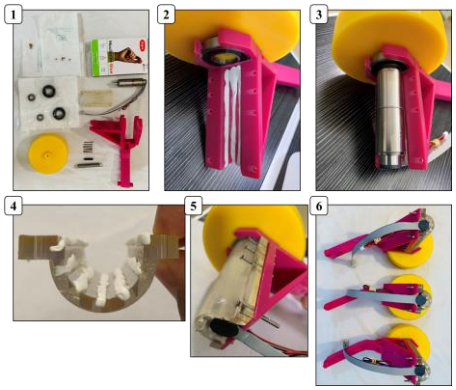

(b)

Fig. 4. Flexible Arm and Actuator. (a) An exploded view of the actuator module. (b) Fabrication steps of the arm and its prototype.

D. Health Issues Considerations in Design

The whole body of the robot prototype is shown in Fig. 5. Since the robot operates in potable water pipelines, it should not be a source of toxic substances. The following considerations were taken to prevent the robot from releasing contaminants.

- The ball bearings are sealed.
- The battery and the actuator module are sealed with moldable glue that isolates them water. Also, the battery is waterproof by manufacturer design.
- The moldable glue becomes solid after 24 hours. According to information provided by the glue manufacturer, it does not include toxic materials.
- Since the sensing and control module is sealed, the electronic components inside the sphere are isolated from outside water.

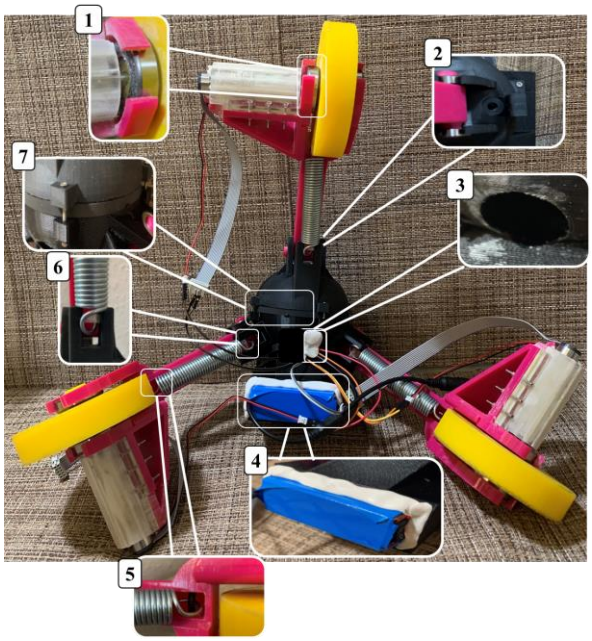

Fig. 5. A draft prototype of the robot. (1) Wheel and motor connection. (2) Water inlet hole. (3) A hole for directing wires into the sphere. (4) Battery. (5) Spring anchor on the arm. (6) Spring anchor on the arm. (7) Sphered sealing mechanism.

III. ROBOT CHARACTERIZATION

A. Static Force Analysis

In this section, forces applied to the robot during an operation in a pipe are simulated and analyzed. This *"static"* analysis helps to estimate the maximum required motor power and spring stiffness. Fig. 6 shows forces acting on the robot, assuming that the robot is moving against the water flow. V_f and V_r are flow and robot velocities, respectively. F_{drag} is the drag force that applies to the robot due to a relative velocity between the robot and the water flow, and it is:

$$\vec{F}_{drag} = \frac{1}{2} m C_D \rho A V_{rel}^2 \quad (1)$$

where m, C_D, ρ, and A are the robot mass, drag coefficient, water flow density, and cross-sectional area. V_{rel} is:

$$V_{rel} = V_r - V_f \quad (2)$$

F_1, F_2 and F_3 are the forces generated by the electric motors. Considering the static forces balance:

$$\vec{F}_{drag} = \vec{F}_1 + \vec{F}_2 + \vec{F}_3 \quad (3)$$

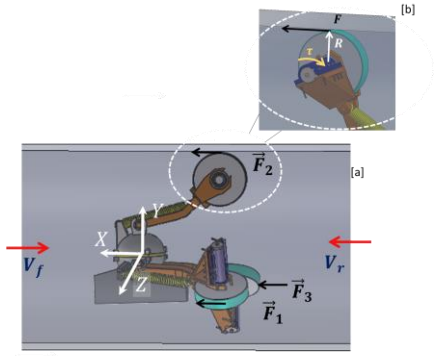

Fig. 6. Forces acting on the robot.

B. Flow Considerations in the Robot Design

Based on the water network topologies, in the majority of the robot operation, it should move horizontally, and the dominant force acting on the robot is the drag force and it is variable. To compute the maximum drag force, a worst-case scenario was defined as follows. The robot is supposed to move against the water flow with a velocity of 0.10 (m/s), and the flow speed is 0.6 (m/s) that is the common flow velocities in water pipelines [29]. A flow simulation model was developed in SolidWorks, and the drag force in the scenario was calculated (see Table II). Since the drag force increases with an increase in the cross-sectional area of a moving object, to compute the maximum drag force, the robot was simulated in its fully open condition where it covers a pipe with a 55.88 (cm) __22 (in)__ diameter (Fig. 7).

TABLE II. SPECIFICATIONS OF THE FLOW SIMULATED IN SOLIDWORKS

Specification [unit]	Value
Fluid type	Water
Fluid pressure [kPa]	413
Fluid density [kg/m^3]	1000
Fluid velocity [m/s]	0.6
Robot velocity [m/s]	0.1
The relative direction of the robot and flow	Opposite

Fig. 7 shows the CFD simulation results. The colors show the relative flow velocity in the pipe and in the vicinity of the robot where water pressure is 413 (kPa), and the flow velocity is – 0.60 (m/s). The largest velocity, shown in blue, is – 0.7 (m/s), which is the relative velocity of the flow to the robot.

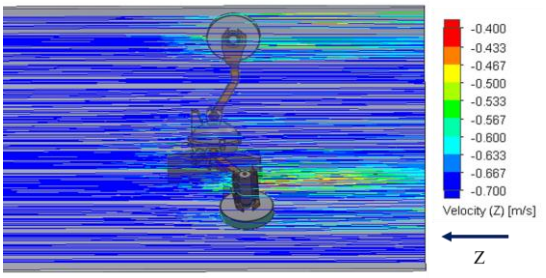

Fig. 7. Flow velocity simulation around the robot to compute the drag force.

Based on the flow simulation, the maximum drag force is approximately 6 (N), which the motors should provide for the robot in the presented extreme condition. Assuming the motors provide the same forces, maximum required force, F_{max}, that each motor should provide is 2 (N), and the maximum torque is:

$$\|\vec{\tau}_{max}\| = \|\vec{F}_{max}.\vec{R}\| \approx 97 \text{ mN.m} \quad (4)$$

Where $\vec{R}$ is the distance vector from the center of each wheel to the force point of action (see Fig. 6). Fig. 7 also shows that the robot is minimally invasive to the flow during operation.

C. *Motor and Gearhead*

Table III shows the characteristics of the customized Maxon motor along with a gearhead for torque amplification and also the encoder.

TABLE III. SPECIFICATION OF THE MOTOR (DCX22L), THE GEARHEAD (GPX22UP) AND THE ENCODER (ENX 16 EASY)

Specification [unit]	Value
Nominal voltage [V]	12
Diameter [mm]	22
Length [mm]	92
Nominal torque at motor shaft[mN.m]	791
The reduction ratio of the gearhead	26:1
Number of motors in the robot	3
# of counts per turn for the encoder	1024
# of channels in the encoder	3

C. *Power Supply*

The power supply is one of the most critical modules for inline robots that have not yet been addressed properly. The available robots designed for pipelines are either tethered [20][30][31] or powered with large portable batteries [19]. The battery specifications are presented in Table IV. The drawn current by motors based on the motor's operating point (provided by the manufacturer) is 0.6 (A). The discharge time of the battery is measured by some experiments and the results demonstrate the duration at which the robot can operate inside the pipeline is more than 3 hours which is enough for one inspection duration. It worth mentioning that the other electrical components consume less power (in the order of milliwatts (mW)) compared to the electrical motors (in the order of Watt (W)) and can be ignored in power profiling calculations.

TABLE IV: SPECIFICATION OF THE SELECTED BATTERY

Specification [unit]	Value
Model	Super polymer lithium-ion
Nominal capacity[A.h]	18
Nominal voltage [V]	11.2
Weight[kg]	0.273
Dimension[mm]	127×65×22

IV. DYNAMIC MODELING AND CONTROLLABILITY

So far, the design, fabrication, and characterization of the robot are presented. In this section, the dynamic equations of the robot are derived, and its controllability and observability are investigated.

A. *Degrees of Freedom (DOF) of the Robot*

The robot DOFs are shown in Fig. 8. The motion in the *z*-axis and the *y*-axis directions and the angular motion around the *x*-axis are constrained in 3D space. So, the robot orientation and position can be represented with $[x \ \emptyset \ \Psi]^T$. The design and placement of the actuators enable the robot to have both translational and rotational motion in a straight path, bends, and Tees.

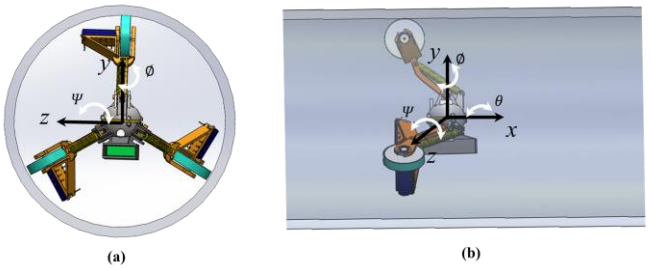

Fig. 8. The robot DOF representation. (a) Front view. (b) Side view.

B. *Dynamic Modeling*

1) *Governing Dynamic Equations*

Based on the frame of reference shown in Fig. 9, motion equations can be written as:

$$\sum_x \vec{F} = m\ddot{x} \rightarrow F_1 + F_2 + F_3 \mp F_{drag} = m\ddot{x} \quad (5)$$

Where F_1, F_2, and F_3 are forces generated motors (see Fig. 6) and computed as:

$$F_i = \frac{\tau_i}{R} \quad i = 1,2,3 \quad (6)$$

Whee τ_i are torques (see Fig. 6). $\ddot{x}$ is the robot acceleration and m is the robot mass. Also, the drag force can be applied in or opposite the robot direction. Therefore, the force can be additive or subtractive in Eq. 5. [see Fig. 6, and Fig. 9]

$$\sum M_y = F_3 L\cos(\theta_3(t,\mathrm{D}))\cos\frac{\pi}{6}\ F_2 L\cos(\theta_2(t,D))\cos\frac{\pi}{6} = I_{yy}\ddot{\emptyset} \quad (7)$$

$$\sum M_z = F_3 L\cos(\theta_3(t,D))\cos\frac{\pi}{3} + F_2 L\cos(\theta_2(t,D))\cos\frac{\pi}{3} - F_1 L\cos(\theta_1(t,D)) = I_{zz}\ddot{\Psi} \quad (8)$$

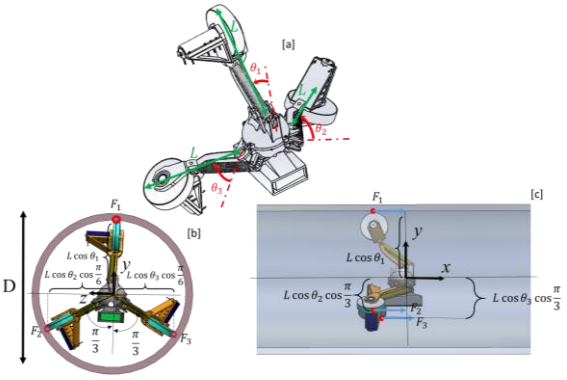

Fig. 9. The robot geometry to derive the governing equations. (a): $\theta_i,\ i = 1,2,3$, is the angle between the spring's neutral axis, where the spring is at normal condition (dashed red line), and the axis where the spring is stretched (solid green line). (b) Front view. (c) Side view.

2) Linearization

Since the stiffness of the springs is the same, and the water pressure is uniform, it can be assumed that the sphere remains at the center of the pipe during the operation. So the angles at (a) in Fig. 9 are equal. Also, they vary when the pipe diameter changes. Hence:

$$\theta_i(t,D) \approx \theta_i(D),\ i = 1,2,3 \quad (9)$$
$$\theta_1(D) = \theta_2(D) = \theta_3(D) \quad (10)$$

3) State-space Representation

The states of the robot based on Eq. [5-10] are:

$$\mathbf{X} = \begin{bmatrix} x_1 = x \\ x_2 = \dot{x}_1 \\ x_3 = \emptyset \\ x_4 = \dot{x}_3 \\ x_5 = \Psi \\ x_6 = \dot{x}_5 \end{bmatrix} \quad (11)$$

The state-space representation of the robot can be represented as:

$$\dot{\mathbf{X}}_{6\times1} = \mathbf{A}_{6\times6}\mathbf{X}_{6\times1} + \mathbf{B}_{6\times3}\mathbf{u}_{3\times1} \quad (12)$$
$$\mathbf{Y}_{6\times1} = \mathbf{C}_{3\times6}\mathbf{X}_{6\times1} \quad (13)$$

where system matrices are as follows.

$$\mathbf{A} = \begin{bmatrix} 0 & 1 & 0 & 0 & 0 & 0 \\ 0 & 0 & 0 & 0 & 0 & 0 \\ 0 & 0 & 0 & 1 & 0 & 0 \\ 0 & 0 & 0 & 0 & 0 & 0 \\ 0 & 0 & 0 & 0 & 0 & 1 \\ 0 & 0 & 0 & 0 & 0 & 0 \end{bmatrix} \quad (14)$$

$$\mathbf{B} = \begin{bmatrix} 0 & 0 & 0 \\ \frac{R}{m} & \frac{R}{m} & \frac{R}{m} \\ 0 & 0 & 0 \\ 0 & -\varphi_1\cos\theta_2 & \varphi_1\cos\theta_3 \\ 0 & 0 & 0 \\ -\varphi_3\cos\theta_1 & \varphi_2\cos\theta_2 & \varphi_2\cos\theta_3 \end{bmatrix} \quad (15)$$

where $\varphi_1 = \frac{\sqrt{3}RL}{2I_{yy}}$, $\varphi_2 = \frac{RL}{2I_{zz}}$, and $\varphi_3 = \frac{RL}{I_{zz}}$.

$$\mathbf{u} = [\tau_1\ \tau_2\ \tau_3]^T \quad (16)$$

$$\mathbf{C} = \begin{bmatrix} 0 & 1 & 0 & 0 & 0 & 0 \\ 0 & 0 & 0 & 1 & 0 & 0 \\ 0 & 0 & 0 & 0 & 0 & 1 \end{bmatrix} \quad (17)$$

The parameters for dynamic modeling of the robot are listed in TABLE V. Now, with the system matrices, we can investigate the system controllability and observability of the system which are two important factors in motion control.

TABLE V. ROBOT PARAMETERS

Variable Name [unit]	Value
m [kg]	2.31
I_{yy} [kg.m^2]	0.0126
I_{zz} [kg.m^2]	0.0093
L [cm]	20
R [cm]	5

4) Controllability and Observability

The system is controllable means that it is possible to reach any final states from initial states by changing the inputs of the system in a finite time. Derivation of the controllability matrix is a cumbersome task and we skip it here for simplicity. The robot is CC (the controllability matrix is full rank). So, with this special placement of the actuators, considering the states, the system is fully *controllable and all maneuverable*. The observability criterion defines how well we can infer the internal states by measuring the outputs. To make the system observable and also remove the hardware complexity, we need to have measurements of the *critical* states and estimate the rest of them based on them. The critical states are the states that if they are not controllable or observable, then the whole system is uncontrollable /unobservable. Here, the critical states are $\dot{x}, \dot{\emptyset}$, and $\dot{\Psi}$ and the other states can be computed by a simple integration of the critical states. To measure the critical states, we need to put a wheel encoder to measure the wheels' angular velocity, and as a result, the translational velocity, $\dot{x}$, and for $\dot{\emptyset}$, and $\dot{\Psi}$, we need an Inertial Measurement Unit (IMU) at the center of the sphere where the coordinate is placed (see Fig. 9). The system is both controllable and observable. So, it is input-observable which means changes in inputs of the robot are reflected in the system measurements.

V. Simulation and Experimental Results

A. Simulation

In this section, the functionality of the robot design presented in the previous sections is evaluated with simulation and experimental results. The robot and its motion were simulated in ADAMS. We analyzed the functionality of the

robot with different equal voltages on motors and evaluated its motion in a straight pipe. Fig. 10, and Fig. 11 show the simulation results. The axes in the diagrams are according to the coordinate system shown in Fig. 9.

Fig. 10 shows the robot velocity during the time, with different voltages on each wheel (the voltages are equal for all wheels). The robot's velocity change is higer in the beginning, but it becomes almost zero for the rest of the time (this is because in the simulation, the wheels are not in contact with the pipe wall at the beginning of the simulation). Therefore, the robot can move smoothly enough to reach maximum velocity in a straight pipe.

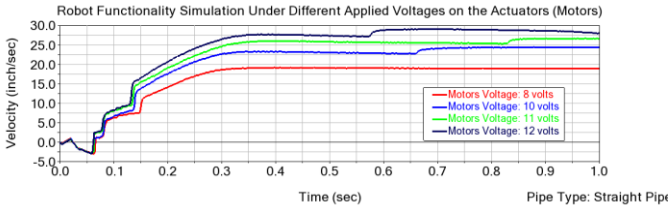

Fig. 10. Robot velocity during the time with different voltages on each wheel.

Fig. 11 shows the angular velocity of the robot about X, Y, and Z axes. Based on Fig. 11, except for the very beginning of the robot motion, the angular velocities change between – 0.3 (revolutions/s) to + 0.3 (revolutions/s). The angular velocity along the pipe axis (X-axis) is minimum compared to other axes (Y and *Z*). In other words, the robot moves with the least rotation about the pipe axis and the maximum rotation about the vertical axis, i.e., axis Y.

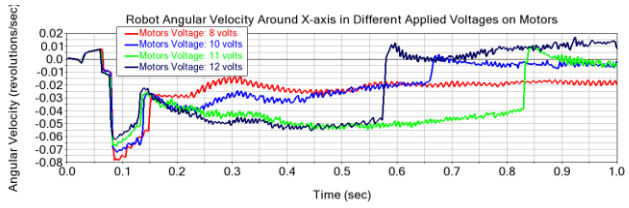

(a)

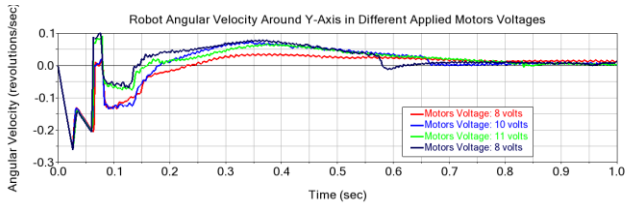

(b)

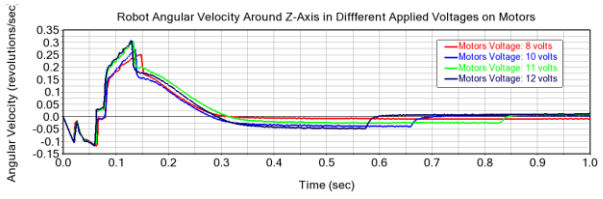

(c)

Fig. 11. Angular velocity of the robot about its axes for different motor voltages. (a) X-axis. (b) Y-axis. (c) Z-axis.

The simulation results show the stable motion of the robot in the pipeline with different equal voltages on the motors. In the next section, the functionality is evaluated by the experiment.

B. Experiment

In this section, we tested the prototyped robot in a straight pipe with 60 inches length and 14 inches diameter. We actuated the robot using the selected battery. The motion of the robot in the pipe is shown by a series of screenshots in Fig. 12. The wheels, in contact with the pipe wall, stabilize the robot during a motion. The maximum velocity measured by the experiment is approximately 1.6 (m/s). The robot also could reach different velocities by changing the duty cycle of the output Pulse Width Modulation (PWM) signal. The robot's functionality was also tested in an upward vertical direction. The experiment showed the robot could move smoothly against its weight force and reach a maximum velocity of about 0.9 (m/s).

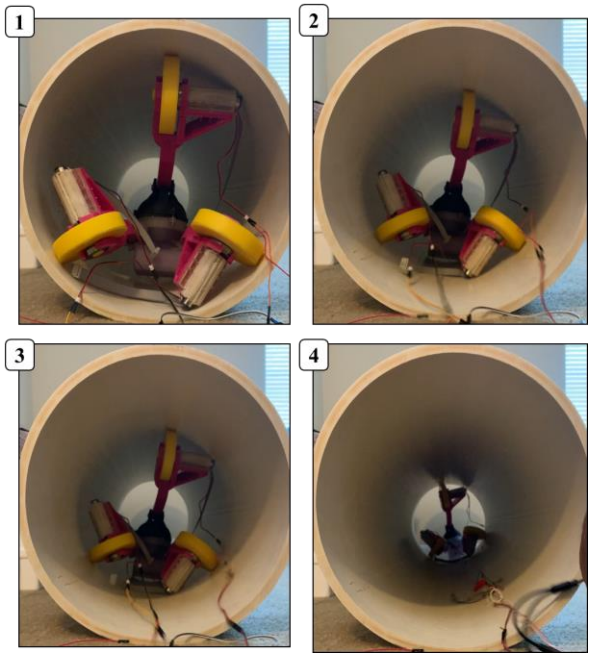

Fig. 12. A series of screenshots showing the robot functionality in the straight pipe with 14 inches diameter.

The robot's operation duration was also verified that turned out to be at least 3 hours by experiment.

VI. Conclusion and Future Works

In this paper, a conceptual design of a modular mobile wall-press robot powered with a hugged-up battery is presented. The robot is capable of embedding miniaturized water quality sensors, motion control unit, and a wireless communication module in Water Distribution Systems (WDSs). The design covers larger pipe diameter ranges of 9 inch- 22 inch. The adjustable arm modules enable the robot to move through straight pipelines with different diameters, in addition to junctions and elbows. The dynamic equations of the robot are derived and the system matrices are presented with linearizations of the dynamic equations. The controllability and observability of the robot showed that the robot is input-observable in which the inputs to the system can

be measured from the output. The robot is also characterized based on Computational Fluid Dynamics (CFD) results considering an extreme condition. As the robot works in potable WDS, health issues are considered in the design, and a prototype is built. The robot performance was analyzed with simulation and experimental results. The simulation results showed a smooth motion inside the pipe. Also, the experiments showed a stable motion inside The pipe. the maximum velocity in which the robot could reach is measured to be 1.6 (m/s) which is much higher than similar works. The robot operation duration is at least 3 hours (based on experiments1), long enough for water quality monitoring tasks in pipes. We also tested the robot in a vertical direction. It could combat its weight and reach a velocity of 0.9 (m/s). In future work, we will design and implement a control algorithm, based on the input-output architecture developed in this paper, which enables the robot to turn towards the desired direction at junctions, where there are multiple paths to choose from. Also, we will develop and add a bi-directional wireless communication module to the robot that will enable it to transceive real-time sensor data and motion control commands between the robot and stationary transceiver units on a pipeline.

REFERENCES

[1] ASCE's 2017 Infrastructure Report Card, *https://www.infrastructurereportcard.org/wp-content/uploads/2017/01/Drinking-Water-Final.pdf.*

[2] U.S. Environmental Protection Agency, National Primary Drinking Water Regulations, *Office of Ground Water and Drinking Water, Washington DC., 2009.*

[3] P. Juuti, H. Mattila, R. Rajala, K. Schwartz, C. Staddon, *Resilient Water Services, and Systems: The Foundation of Well-Being.* International Water Association, 2019, pp. 54–67.

[4] A. Selvakumar, A. Tafuri, "Rehabilitation of Aging Water Infrastructure Systems: Key Challenges and Issues," *Journal of Infrastructure Systems*, vol. 18, pp. 202–209, 2012.

[5] A. Selvakumar, J. Matthews, W. Condit, and R. Sterling, "Innovative research program on the renewal of aging water infrastructure systems," *Journal of Water Supply: Research and Technology-Aqua*, vol. 64, no. 2, pp. 117-129, 2014.

[6] Utah State University-Buried Structures Laboratory, "Water Main Break Rates in the USA and Canada: A Comprehensive Study," 2018.

[7] U.S. Environmental Protection Agency. Potential contamination due to cross-connections and backflow and the associated health risks. *Office of Ground Water and Drinking Water, Washington DC.*, 2001.

[8] U.S. Environmental Protection Agency. The Standardized Monitoring Framework: A Quick Reference Guide. *Office of Ground Water and Drinking Water, Washington DC.*, 2004.

[9] M. Storey, B. van der Gaag and B. Burns, "Advances in on-line drinking water quality monitoring and early warning systems," *Water Research*, vol. 45, no. 2, pp. 741-747, 2011.

[10] B. Hohman, "Challenge Studies of the Pittsburgh Distribution Network Pilot Contamination Warning System," B.Sc., University of Pittsburgh, 2007.

[11] N. Sankary and A. Ostfeld, "Inline Mobile Sensors for Contaminant Early Warning Enhancement in Water Distribution Systems," *Journal of Water Resources Planning and Management*, vol. 143, no. 2, p. 04016073, 2017.

[12] M. Banks, R. Wu, W. Wan Salim, A. Hermann, R. Staton, and D. Porterfield, "Real-time monitoring of total residual chlorine in water distribution systems based on micro-electro-chemical-sensor," Presented at the Institute of Biological Engineering Annual Conference, Indianapolis, IN, 2012.

[13] D. M. Chatzigeorgiou. Analysis and design of an in-pipe system for water leak detection. *Massachusetts Institute of Technology*, 2010.

[14] Pure Technologies. Smartball for water and wastewater water mains. *https://www.puretechltd.com/technology/smartball-leak-detection/.*

[15] T. Lai, W. Chen, Y. Chen, P. Huang, and H. Chu, "Mapping hidden water pipelines using a mobile sensor droplet," *ACM Transactions on Sensor Networks*, vol. 9, no. 2, pp. 1-33, 2013.

[16] Pure Technologies, Pipediver, *https://puretechltd.com/technology/pipediver-condition-assessment/.*

[17] Pure Technologies, "SmartBall Inspection Report of North Beach Force Main," Pure Americas Inc., 2011.

[18] L. Shao, Y. Wang, B. Guo, and X. Chen, "A review over state of the art of in-pipe robot," 2015 IEEE International Conference on Mechatronics and Automation (ICMA), Beijing, 2015, pp. 2180-2185.

[19] Y. Qu, P. Durdevic, and Z. Yang, "Smart-Spider: Autonomous Self-driven In-line Robot for Versatile Pipeline Inspection," *IFAC-PapersOnLine*, vol. 51, no. 8, pp. 251-256, 2018.

[20] Y. Kwon, B. Yi, "Development of a pipeline inspection robot system with a diameter of 40mm to 70mm", 2010 IEEE International Conference on Mechatronics and Automation, Alaska, 2010, vol. 51, no. 8, pp. 251-256, 2018.

[21] M. M. Moghaddam, S. Jerban, "On The In-pipe Inspection Robots Traversing Through Elbows," *International Journal of Robotics*, vol. 4, no. 2, pp. 19-27, 2015.

[22] A. Kakogawa and S. Ma, "Design of a multilink-articulated wheeled pipeline inspection robot using only passive elastic joints," *Advanced Robotics*, vol. 32, no. 1, pp. 37-50, 2017.

[23] F. B. I. Alnaimi, A. A. Mazraeh, K. Sahari, K. Weria, and Y. Moslem, "Design of a multi-diameter inline cleaning and fault detection pipe pigging device," 2015 IEEE International Symposium on Robotics and Intelligent Sensors (IRIS), Langkawi, 2015, pp. 258-265.

[24] D. Chatzigeorgiou, K. Youcef-Toumi, A. Khalifa, and R. Ben-Mansour, "Analysis and design of an in-pipe system for water leak detection," ASME 2011 International Design Engineering Technical Conferences and Computers and Information in Engineering Conference, Washington DC, 2011, pp. 1007-1016.

[25] M. Abdul Wahed, and M. Arshad. "Wall-press type pipe inspection robot." 2017 IEEE 2nd International Conference on Automatic Control and Intelligent Systems (I2CACIS), Shah Alam, Malaysia, 2017, pp. 185-190.

[26] Pure Technologies, Sahara leak & gas pocket detection, *https://puretechltd.com/technology/sahara-leak-gas-pocket-detection/.*

[27] A. A. Bandala et al., "Control and Mechanical Design of a Multi-diameter Tri-Legged In- Pipe Traversing Robot," 2019 IEEE/SICE International Symposium on System Integration (SII), Paris, France, 2019, pp. 740-745. (Z)

[28] R. Wu, W. Wan Salim, M Razali, J. Park, A. Brovont, A. Pekarek, M. Banks, D. Porterfield. "Development of mobile sensor technology for in-pipe water quality monitoring," Presented at the Institute of Biological Engineering Annual Conference, Lexington, KY, 2014.

[29] Bryan/College Station Water Authorities, "Bryan/College Station Unified Design Guidelines," 2012.

[30] C. Choi, D. Chatzigeorgiou, R. Ben-Mansour, and K. Youcef-Toumi, "Design and analysis of novel friction controlling mechanism with minimal energy for in-pipe robot applications," 2012 IEEE International Conference on Robotics and Automation, 2012, pp. 4118–4123.

[31] K. Miyasaka, G. Kawano, and H. Tsukagoshi, "Long-mover: Flexible Tube In-pipe Inspection Robot for Long Distance and Complex Piping," 2018 IEEE/ASME International Conference on Advanced Intelligent Mechatronics (AIM), 2018, pp. 1075–1080.